Organic Electronics 71 (2019) 136–142

Contents lists available at ScienceDirect

Organic Electronics

journal homepage: www.elsevier.com/locate/orgel

Optical and electrical effects of nanobump structure combined with an undulated active layer on plasmonic organic solar cells

Hyung-Jun Song[a,b,d,1], Gunhee Lee[a,c,1], Kinam Jung[a,c,e], Min Seok Jang[a,f], Jiho Sohn[a,b], Jong-Kwon Lee[a,g,***], Mansoo Choi[a,c,**], Changhee Lee[a,b,*]

[a] Global Frontier Center for Multiscale Energy Systems, Seoul National University, 1-Gwanak-ro, Gwanak-gu, Seoul, 08826, Republic of Korea
[b] Department Electrical and Computer Engineering, Seoul National University, 1-Gwanak-ro, Gwanak-gu, Seoul, 08826, Republic of Korea
[c] School of Mechanical and Aerospace Engineering, Seoul National University, 1-Gwanak-ro, Gwanak-gu, Seoul, 08826, Republic of Korea
[d] Department of Safety Engineering, Seoul National University of Science & Technology, 232 Gongneung-ro, Nowon-gu, Seoul, 01811, Republic of Korea
[e] Department of Mechanical Engineering, Hannam University, 70 Hannamro, Daedeok-Gu, Daejeon, 34430, Republic of Korea
[f] School of Electrical Engineering, Korea Advanced Institute of Science and Technology, Daejeon, 34141, Republic of Korea
[g] Department of Nanostructure Technology, National Nanofab Center, Daejeon, 34141, Republic of Korea

ARTICLE INFO

Keywords:
Organic solar cells (OSCs)
Metallic nano structure
Dielectric layer
Plasmonic effect

ABSTRACT

The effect of nanobump structure (NS) constructed with molybdenum oxide (MoO_3) covering aerosol-derived Ag nanoparticles on organic solar cells is systematically explored by varying the MoO_3 thickness. The amount of enhanced light absorption by the NS-induced scattering and plasmonic resonance effects increases with decreasing MoO_3 thickness. Meanwhile, the oval-shape NS with fully enclosed Ag nanoparticles by MoO_3 leads to significantly improved carrier extraction due to decreased ohmic loss, while the NS with partially covered Ag nanoparticles by thin MoO_3 degrades device performance arising from increased recombination and leakage loss. Thus, the optimal MoO_3 thickness occurs around 20 nm for 40 nm sized nanoparticles where the enhanced carrier generation and the improved carrier extraction by the NS effectively contribute to the improvement in photocurrent. Therefore, our analysis on carrier dynamics of plasmonic organic solar cells incorporating the NS would provide a clear guideline for optimizing device performance.

1. Introduction

Organic solar cell (OSC) is a very promising alternative to conventional inorganic solar cells owing to its commercialization and processing advantages such as low-cost, light-weight, flexible, thin, large-area features, and simple process [1,2]. It is well-known that the power conversion efficiency (PCE) of OSCs is limited by the mismatch between carrier transport scale (~several tens of nanometre) and optical absorption length (< 100 nm) [3]. In this respect, there have been many efforts to harness more light in OSCs without deteriorating their electrical properties [4–7]. Among these, implementing noble metallic nanoparticles (NPs) in OSCs is a very efficient strategy to enhance light harvesting induced by plasmonic effect. Here, the increased absorption from localized surface plasmon resonance near NPs and the elongated optical paths for incident light by scattering lead to the outstanding improvement in PCE of single and tandem OSCs [4,7–11]. Also, NPs have been exploited to achieve electrical enhancement by using their high carrier mobility and well-aligned energy levels with an active material, which effectively transports generated carriers into electrodes with small losses [12]. Meanwhile, the surface texture of nanostructured electrodes or buffer layers in OSCs has been used to increase light absorption inside active layer by the multiple reflection and grating effect [8,13–15]. Here, the enlarged interface area between an active layer and a buffer layer also provides a significant enhancement in PCE owing to improved carrier swept-out to electrodes [12].

However, the role of NPs and nanostructures is still a controversial issue, because the increased absorption inside active layer by them is not always channelled into highly efficient devices [16,17]. According to previous reports, unfilled polymer voids formed in a height-modulated active layer by underlying nanostructures degrade the device

* Corresponding author. Global Frontier Center for Multiscale Energy Systems, Seoul National University, Seoul, 08826, Republic of Korea.
** Corresponding author. Global Frontier Center for Multiscale Energy Systems, Seoul National University, Seoul, 08826, Republic of Korea.
*** Corresponding author. Global Frontier Center for Multiscale Energy Systems, Seoul National University, Seoul, 08826, Republic of Korea.
E-mail addresses: jklee7@nnfc.re.kr (J.-K. Lee), mchoi@snu.ac.kr (M. Choi), chlee7@snu.ac.kr (C. Lee).
[1] These authors contributed equally to this work.

https://doi.org/10.1016/j.orgel.2019.05.007
Received 15 October 2018; Received in revised form 2 April 2019; Accepted 7 May 2019
Available online 11 May 2019

performance [18]. Additionally, a direct contact between polymer layers and NPs may promote non-radiative energy transfer among them, which generally increases exciton quenching [19]. Moreover, the reduced charge collection in OSCs including NPs is exhibited from metal-mediated recombination losses [16,17,20]. Considering the aforementioned effects of nanostructures on PCE enhancement or detraction of OSCs, dielectric encapsulated nanostructures have been suggested to maximize device performance by reducing exciton quenching or recombination losses [21,22]. Nevertheless, these proposed methods also have a similar problem, the existence of competition between optical field enhancement and carrier annihilation by them [17]. Besides, to date, the effect of encapsulation layer's thickness on the performance of OSCs has not been systematically analysed, despite its importance. Thus, it is imperative to analyse the effect of plasmonic structures consisting of encapsulated NPs or nanostructures to enhance the device performance in optical and electrical aspects.

In this study, the plasmonic nanobump structure (NS), constructed with thermally evaporated MoO_3 covering aerosol-derived Ag NPs, is adopted to systematically explore the effect of MoO_3 thickness (t_M) on carrier generation and extraction in the device. By varying the t_M from 5 to 30 nm, the NS including 40 nm-sized NPs has different oval-shapes protruded into the active layer and the encapsulated status of NPs is controlled. The PCE of OSCs embedding the NS with t_M of 20–30 nm is improved and the best performance (14% enhancement) is achieved at t_M of 20 nm, whereas the devices with partially uncovered Ag NP by a thin t_M of 5–10 nm show lower efficiency compared to those with flat MoO_3 layer. The underlying mechanism of enhanced or degraded performance of the device embedding the NS with different t_M is analysed by optical and electrical characterizations through UV–visible spectroscopy, optical simulation, photoluminescence (PL), current density-voltage (J-V), and capacitance-voltage (C–V) measurements. As a result, we have successfully clarified the role of NS on the device performance in terms of the enhanced light harvesting, exciton quenching, and recombination losses, which allows us to find the optimized device structure for highly efficient OSCs.

2. Experimental

The schematic of OSCs with NS is shown in Fig. 1a. The Indium tin oxide (ITO) patterned glass was cleaned with isopropyl alcohol and acetone for 15 min and dried in a vacuum oven. The substrate was treated with UV-ozone to remove remaining solvent followed by Ag NPs deposition on the ITO. Here, the precisely size-controlled Ag NPs were generated by an evaporation and condensation method based on aerosol process at ambient pressure [23–25]. Also, the diameter of NPs was fixed at 40 nm, since the most efficient plasmonic effect is occurred at this NP's size according to our previous report [11]. The concentration of NPs is $\sim 0.5 \times 10^9/cm^2$, which is estimated from field emission scanning electron microscopy images (AURIGA, Carl Zeiss). To elucidate the effect of t_M on OSCs, MoO_3 with different thickness (5–30 nm) was deposited on the Ag NP pre-deposited ITO at a high vacuum chamber ($< 5 \times 10^{-7}$ Torr), which results in the formation of NS. Then, 100 nm of polymer blend in dichlorobenzene (25 mg mL-1), poly [N-9″-hepta-decanyl-2,7-carbazole-alt-5,5-(4′,7′-di-2-thienyl-2′,1′,3′-benzothiadiazole) (PCDTBT) and [6,6]-phenyl C70 butyric acid methyl-ester ($PC_{70}BM$) (1:4, weight ratio), was spin casted on the NS. The coated film was annealed 2 h in a high vacuum chamber to remove remaining solvents. After that, 0.5 nm of LiF and 100 nm of Al were sequentially deposited by thermal evaporation method. To investigate the effect depending on the thickness variation of buffer layer, we also fabricated reference devices including the same t_M without NPs as the devices embedding NS. All the fabrication processes were performed in a nitrogen filled glove box and a high vacuum chamber. Hereafter, we denote the NS with d nm t_M as NS-d and the flat buffer layer with the same thickness as flat-d.

The J-V characteristics were measured by using a Keithley 237 source measurement unit under dark and AM 1.5G illumination condition at an intensity of 100 mW/cm^2 with an Oriel S013ATM solar simulator, calibrated by a standard silicon reference solar cell (91150V, Newport). The accuracy of measurement is re-examined by comparing photocurrent density of device and integration of its external quantum efficiency under AM 1.5 G condition. In addition, the neutral density filter was used to investigate the light intensity dependence of device performance. To calculate carrier density and recombination losses, the C–V characteristics of devices under dark condition were measured from −1.2–1.2 V at 100 kHz using an impedance analyser (4192A, Agilent technologies). For analysing plasmonic effect induced by NS, the absorption of PCDTBT:$PC_{70}BM$ film with NS was measured depending on different t_M. In addition, the films on flat buffer layer with the same t_M as the NS were also analysed to remove side effects such as the change of transmittance and reflectance of ITO/MoO_3 substrate caused by the different thickness of dielectric layer. These were performed using the Cary 5000 UV–Vis–NIR spectrophotometer (Agilent Technologies) with integrating sphere system. Furthermore, the steady-state and time resolved PL excited by 405 nm laser diode were recorded using iHR320 (Horiba, Ltd.).

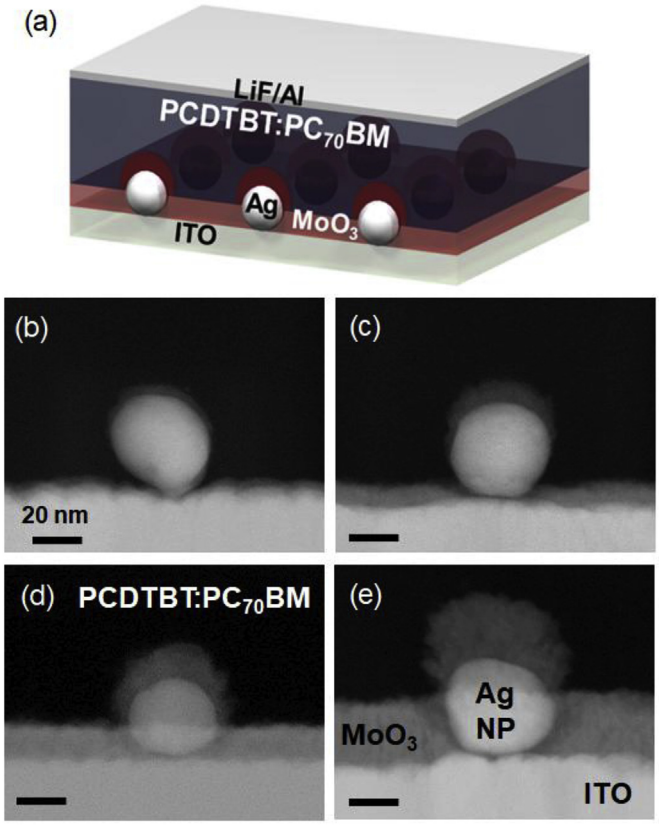

Fig. 1. (a) Schematic of OSCs with NS. Cross-sectional TEM images of OSCs including NS with different t_M: (b) 5, (c) 10, (d) 20, and (e) 30 nm.

3. Results and discussion

3.1. Nano-morphology of NS

To verify the nano-morphology and encapsulating status of NS depending on t_M, transmission electron microscopy (TEM) analysis of OSCs was performed. Fig. 1b–e shows cross-sectional TEM images of NS-5, 10, 20, and 30. The upper parts of NPs in NS-5 and 10 are fully covered by MoO_3, while the *sides* of them are partially disclosed into the polymer blend. Here, approximately 60% and 25% of NP's surface area are exposed to the polymer blend in the NS-5 and 10, respectively. On

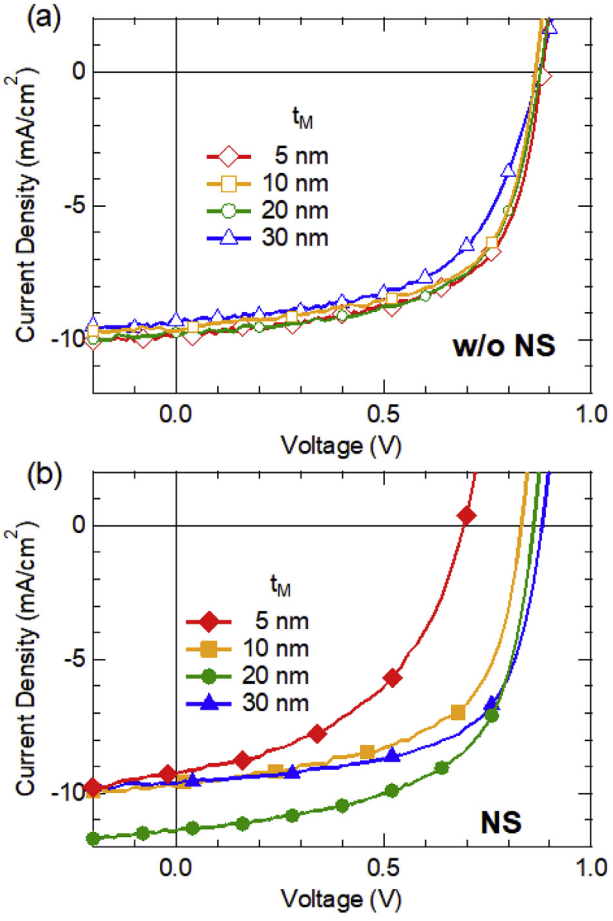

Fig. 2. J-V Characteristics of OSCs (a) without and (b) with NS employing different t_M.

the other hand, NPs in NS-20 and 30 are fully isolated from the active layer, with minimum MoO_3 thickness of 4 and 7 nm, respectively. Also, the upper parts of them are covered with the same thickness as the t_M directly deposited on the ITO layer. The shape of NS is close to an oval structure caused by the shadowing effect of thermal deposition process during MoO_3 formation on the pre-deposited NPs. This analysis guarantees that the encapsulation status of NPs can be tuned by controlling t_M, which is difficult to realize for the case of solution process.

3.2. Device performance of OSC with NS

Fig. 2 and Table 1 show the device performance of OSCs with and without NS employing different t_M. Device parameters of OSCs without NS, short circuit current density (J_{SC}), open circuit voltage (V_{OC}), fill factor (FF), and PCE, are in a similar range when the t_M is thinner than 20 nm. In contrast, the PCE of device including flat-30 (4.61%) slightly decreases due to reduced FF (0.58). For the case of NS incorporated devices, the PCE of OSCs with NS-20 (5.79%) is enhanced compared to that with flat-20 (5.12%) as a consequence of increased photocurrent. And, the improvement in FF of device with NS-30 (0.62) leads to better device performance (PCE of 5.11%) than that of OSCs with flat-30. Hence, the improvement in the PCE of OSC is achieved by adopting NPs fully enclosed by t_M less than 30 nm. Meanwhile, in spite of enlarged interface area between the active layer and the buffer layer from NS, PCEs of OSCs containing incompletely encapsulated NPs, (NS-5: 3.30% and NS-10: 4.70%) decrease in comparison with those of OSCs including the same flat-d without NPs. This low PCE of these samples is attributed to decreased FF and V_{OC} without any enhancement in J_{SC}. Especially, these photovoltaic parameters of OSCs embedding partially

Table 1
Device performance of the OSCs with and without NS employing different thickness of MoO_3 (t_M), where the average and standard deviation values of the device parameters are presented. Here, the average and standard deviation values were derived from 5 different samples.

t_M	Device	J_{SC} (mA/cm^2)	V_{OC} (V)	FF	PCE (%)
5 nm	Flat	9.61 ± 0.18	0.88 ± 0.01	0.62 ± 0.01	5.24 ± 0.18
	NS	9.22 ± 0.13	0.70 ± 0.03	0.50 ± 0.04	3.30 ± 0.28
10 nm	Flat	9.55 ± 0.09	0.87 ± 0.01	0.61 ± 0.01	5.11 ± 0.04
	NS	9.61 ± 0.18	0.84 ± 0.02	0.58 ± 0.01	4.70 ± 0.21
20 nm	Flat	9.58 ± 0.15	0.87 ± 0.01	0.61 ± 0.01	5.12 ± 0.13
	NS	11.13 ± 0.24	0.87 ± 0.01	0.60 ± 0.01	5.79 ± 0.13
30 nm	Flat	9.19 ± 0.13	0.86 ± 0.01	0.58 ± 0.01	4.61 ± 0.13
	NS	9.34 ± 0.24	0.87 ± 0.01	0.62 ± 0.01	5.11 ± 0.27

encapsulated NPs ($t_M \leq 10$ nm) degrade, as the t_M decreases. This result is inconsistent with previous reports about the interaction between NPs and organic semiconducting materials demonstrating that the exciton generation increases as the distance between NPs and organic material decreases [22,26,27]. To find out the origin of this discrepancy, the electrical and optical effects of NS on OSCs were systematically studied in aspects of exciton generation, exciton lifetime, and carrier transport.

3.3. Exciton generation

To explore how the NSs affect light absorption characteristics of the device, we compared UV–visible absorption spectra of polymer blend films with and without NS, as presented in Fig. 3a. In all cases, films including NS consistently absorb more light compared to flat films with the same t_M within 450–650 nm wavelength range, where plasmon resonance of NPs takes place. As a quantitative measure of absorption enhancement induced by the NS, we evaluated the integrated enhancement factor, defined as the relative increase of the total absorption in the films with NS-d compared to those with flat-d within PCDTBT: $PC_{70}BM$ absorption band (380–720 nm) under AM 1.5G illumination (Fig. 3b). For all the samples, the absorption enhancement factors are positive, clearly indicating the inclusion of NSs is beneficial in terms of exciton generation. The enhancement factor, however, decreases from 11% to 3% as t_M increases from 5 nm to 30 nm.

In order to explain the origin of the absorption enhancement induced by the NSs, we performed electromagnetic simulations using the finite-difference time-domain (FDTD, Lumerical) method, which demonstrates the effects of scattering and local electric field enhancement due to the plasmon resonance of the embedded Ag NPs. The scattering by NS is distinctly enhanced in 450–650 nm wavelength (See Fig. S1a), which coincides with the absorption enhancement of films with the NSs. Here the scattering intensity of all the samples are in the similar level regardless of the thickness of the encapsulating layer because of modest difference in refractive indices of MoO_3 and PCDTBT:$PC_{70}BM$. On the other hand, the enhancement in electric field near the NPs associated with localized surface plasmon resonance (LSPR) only reaches in the vicinity of them. The LSPR induced by NS exponentially decays as it goes farther from the metal surface with the characteristic length of a few tens of nano meters as shown in Fig. 3c [28]. Therefore, the absorption enhancement due to the local field enhancement decreases with increasing t_M as the smaller volume of the active material is included in the effective region, which agrees with the downward trend observed in Fig. 3b. Recognizing that light absorption mainly occurs in the active layer by generating excitons, the measured enhancement in J_{SC} of NS-20 and 30 is attributed to the optical absorption enhancement by plasmon resonances. However, in the devices with thinner encapsulation layer (NS-5 and 10), the improved exciton generation fails to increase J_{SC}, and we believe this cannot be explained solely by

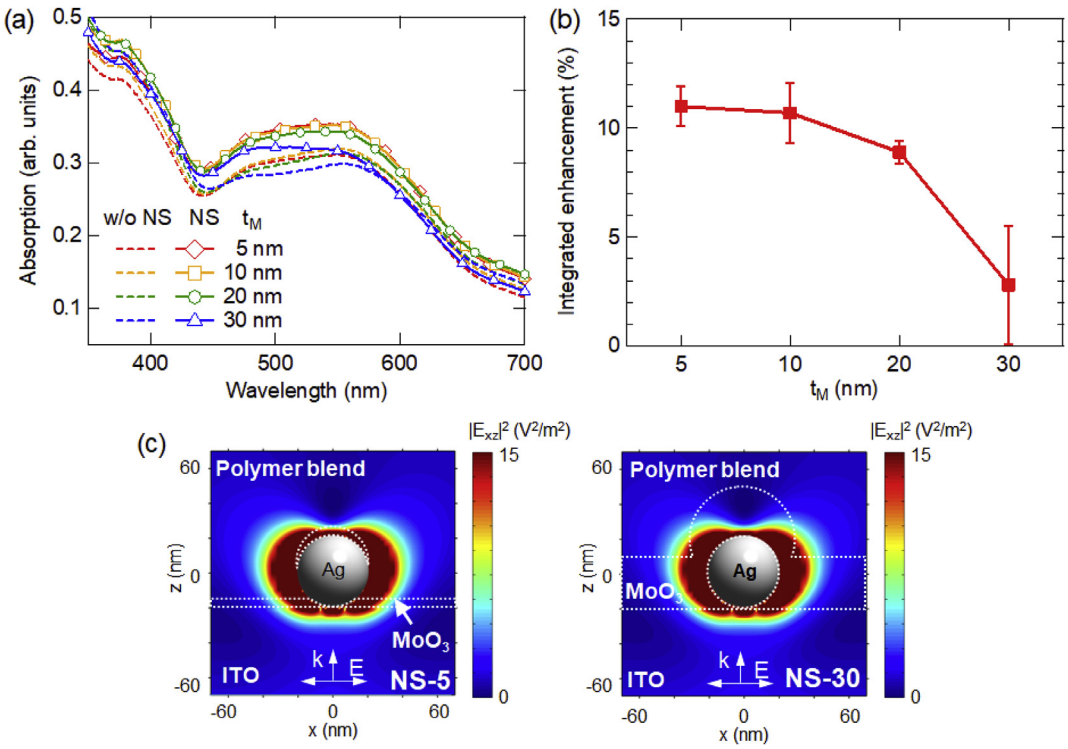

Fig. 3. (a) Absorption of films (~40 nm, PCDTBT:$PC_{70}BM$) with and without NS. (b) Integrated absorption enhancement of films (weighted solar spectrum based on AM 1.5 G) with NS compared to case with flat as a function of t_M. The average and standard deviation of the ratio are achieved from 7 different batches. (c) Electric field distribution (λ = 550 nm, xz plane) of film with NS-5 and 30. Here, the absorption coefficient (k) of all layer is fixed 0 to remove side effect from the variation NS's volume due to different t_M.

optical analysis. In the next session, we investigate the electrical properties of our devices revealing that the imperfect encapsulation of Ag NPs leads to severe exciton quenching.

3.4. Exciton lifetime

To clarify why the increased absorption of films with partially covered NPs does not affect J_{SC}, the exciton generation and quenching in films with NS depending on the t_M was studied using PL of donor only film excited by 405 nm wavelength laser diode. The samples for PL measurement were prepared by spin-coating of PCDTBT layer (~40 nm) onto MoO_3 layer with and without Ag NPs. Fig. 4a shows the steady state PL intensity of the four kinds of NS samples compared to one without NS (t_M = 10 nm). The PL intensities increase in a broad range in the film with fully covered NPs (NS-20 and 30), showing a peak at 690 nm wavelength, whereas those of polymer casted on NS-5 and 10 are lower than the case without NS. These results show different tendency from the absorption measurement in that the absorption of all the samples with NSs regardless of t_M is enhanced in comparison with that of the reference ones. The PL intensity is commonly determined by two factors: the decay of photo generated exciton and the frequency overlap between the plasmonic peak of NS and the energy band gap of polymer. Although absorption enhancement induced by the plasmonic NS is in a similar range, PL intensity of films with NS-5 and 10 is lower than that without NS. Hence, it can be inferred that the exciton annihilation plays a role to decrease the steady-state PL intensity due to the direct contact of Ag NPs with polymer in those cases (Fig. 1b and c). [29,30]. Meanwhile, in the films with NS-20 and 30, Ag NPs are fully isolated from the polymer by the MoO_3, the exciton quenching from NPs is negligible compared to the enhanced exciton generation induced by plasmonic effect. Especially, the PL intensity of NS-20 is higher than that of NS-30. As aforementioned, this phenomenon might be attributed to the less amount of exciton in a polymer casted on NS-30 than that on NS-20, because the plasmonic near-field enhancement induced by NS decreases as the distance between the NPs and the polymer increases.

For directly measuring the decay time of exciton in PCDTBT with NS, the exciton lifetime was calculated from time-resolved PL at the wavelength of 690 nm using multi-exponential function as shown in Fig. 4b [31]. The observed lifetime of the polymer with NS-20 and 30 are 520 ± 15 and 531 ± 24 ps, respectively. Interestingly, these values are similar to exciton lifetime of film deposited on the flat buffer layer (520 ± 18 ps). In contrast, excitons in film including the NS–5 and 10 are decayed faster (378 ± 20 and 448 ± 15 ps, respectively). The short lifetime is normally related to non-radiative energy transfer from polymer, so the excitons in films with NS-5 and 10 have more chance of annihilation than the other cases. Therefore, the proper t_M, just fully capping Ag NPs, prevents generated exciton from their annihilation inside device, which results in maximizing the generation of carrier induced by the plasmonic effect from NS.

3.5. Carrier transport: leakage and ohmic losses

Next, we investigate the behaviour of generated carriers swept-out to electrodes in devices with and without NS. In order to analyse losses from leakage paths and contact resistance, the equivalent circuit model was applied to *OSCs* by introducing shunt (R_{SH}) and series (R_S) resistances derived from *entire J-V curve under light irradiation* [32]. Fig. 5 illustrates the R_S and R_{SH} values of OSCs as a function of t_M. It is observed that the R_S of devices without NS increases as t_M increases. Since the interface between the active layer and the cathode (LiF/Al) is maintained the same among the samples, this increase of ohmic losses in OSCs with increasing flat MoO_3 is mainly attributed to reduced carrier swept-out to the anode due to prolonged hole carrier extraction path. Thus, the reduced PCE of OSCs fabricated on the flat-30 can be explained by the increased ohmic losses during carrier transport process, thereby resulting in low FF of the OSC, which is consistent with

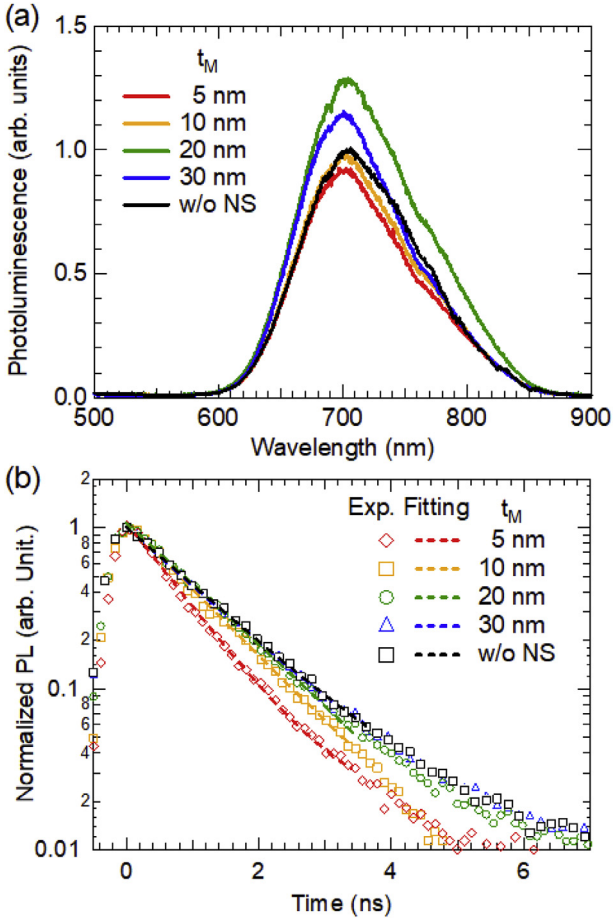

Fig. 4. (a) Steady state PL and (b) Transient PL of PCDTBT films with NS excited by 405 nm laser. The t_M of films without NS was 10 nm.

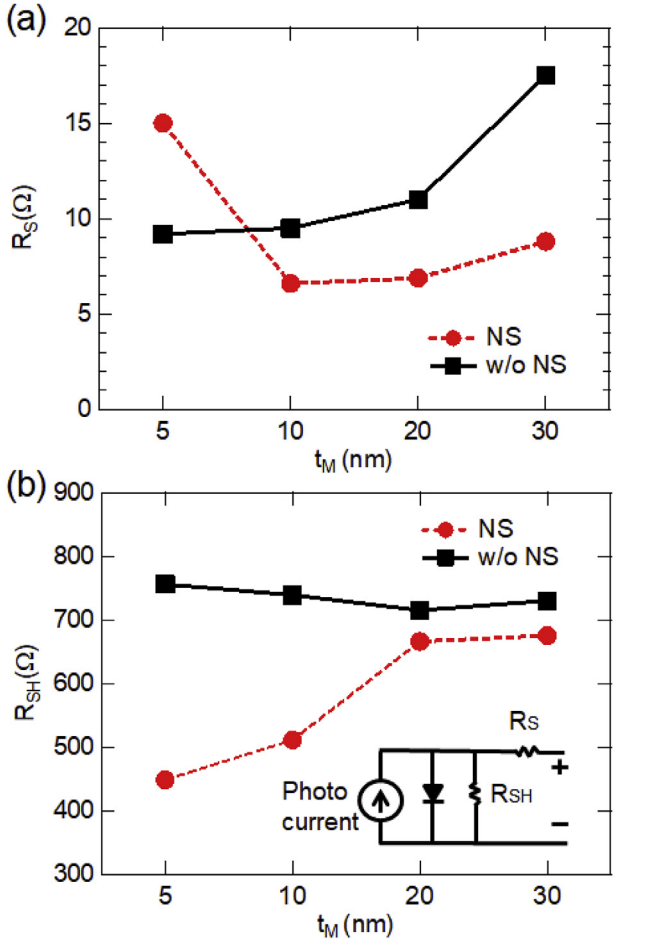

Fig. 5. (a) R_S and (b) R_{SH} of devices with and without NS embedding different t_M. The inset of (b) represents equivalent circuit model for this analysis.

the study of P3HT: $PC_{60}BM$ blends based OSCs with different t_M [33]. In the meantime, the R_S values of OSC with NS-10, 20, and 30 are lower than those of each reference samples including the same t_M. Particularly, these values are lower than the R_S of OSC with flat-5. It means that the insertion of Ag NPs in MoO_3 layer of OSCs leads to significant enhancement in carrier extraction, which is not observed in the *OSC* implementing core/shell type NPs [21,22,34]. We believe that this enhancement is originated by the following three reasons. First, the interface area between an active layer and a hole extraction layer is enlarged due to protruded structure of NS into the active layer, which is favourable to reduce the R_S. On the other hand, in the case of NPs enclosed by dielectric shell and/or covered by solution-processed buffer layer, the hole buffer and active layer maintain a flat structure, where it is difficult to observe the reduced carrier loss happen in the undulated active layer. In addition, the distance between the anode and the active layer in OSCs with NS is effectively shortened compared to the case without NS as shown in Fig. 1. For instance, the side of NP is covered by thinner dielectric layer compared to the targeted deposition thickness, even in cases of fully encapsulated one (NS-20: ~4 nm, NS-30: ~7 nm). It is well-known that the carrier can transport to the electrode with small losses throughout thin dielectric layer less than 10 nm [33]. In the case of core/shell type NPs whose shell's thickness is thicker than tens of nanometre, the enhanced carrier transport is not observed, since the carrier loss monotonically increases as the shell thickness of the dielectric layer increases. Furthermore, the carrier mobility through NPs is much faster than that in MoO_3 and polymer layers, so that the generated carrier can effectively move to the electrode with small ohmic losses [34]. Here, the NPs inside NS are directly contacted with the anode, while NPs are not directly connected with an electrode in a core/shell structure. Thus, the oval-shaped NS enables carriers to be extracted with minimized ohmic losses. Not only reduced R_S, but also enhanced current density at a high forward bias (1 V) is a supportive evidence of decreased ohmic losses in OSCs with NS, in comparison with ones without NS. Here, the R_S of device with NS-5 is higher compared to the other devices, because the J-V curve of it follows the non-ideal diode behaviour, resulting in reduction of slope at V_{OC} (See Fig. S2). Nevertheless, the current density of OSC including NS-5 is much higher than that of one with flat-5 at a high forward bias owing to the aforementioned reasons. Therefore, the enhancement in extraction of generated carrier to electrode is pronounced in the OSCs with NS and undulated active layer, arising from decreased ohmic losses regardless of NP's encapsulation status.

Meanwhile, R_{SH}s of OSCs with uncovered NPs, NS-5 (448 Ω) and 10 (511 Ω), are dramatically reduced in comparison with the cases of flat one (705–756 Ω), as shown in Fig. 5b. On the other hand, R_{SH}s of device with NS-20 (665 Ω) and 30 (675 Ω), including fully covered NPs, are similar to those of device without NPs, despite shortened distance between the anode and the cathode due to embedded NPs [18]. Since the R_{SH} represents leakage features inside devices, these results indicate that partially encapsulated NPs inside OSCs work as leakage paths, while fully covered one does not affect carrier losses from leakage. These properties are also observed in Semi-log J-V plot of OSCs under dark condition (See Fig. S3), which illustrates that the current density of OSC with NS at a reverse bias (−1 V) is inversely proportional to the t_M. It is noted that the two orders of magnitude higher reverse dark current of device with NS-5, in comparison with those embedding NS-20 and 30, is observed. As a result, FFs of devices containing NS-5

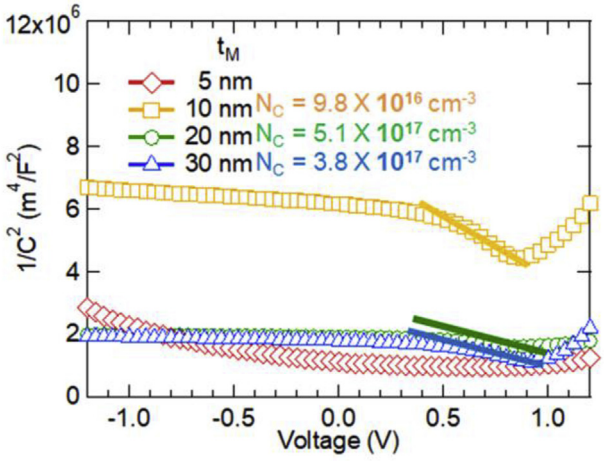

Fig. 6. Capacitance-voltage (C–V) characteristics of OSCs under dark condition. The graph indicated that the carrier density decreased in the device with partially covered NPs, while the device with thick buffer layer maintained its carrier density.

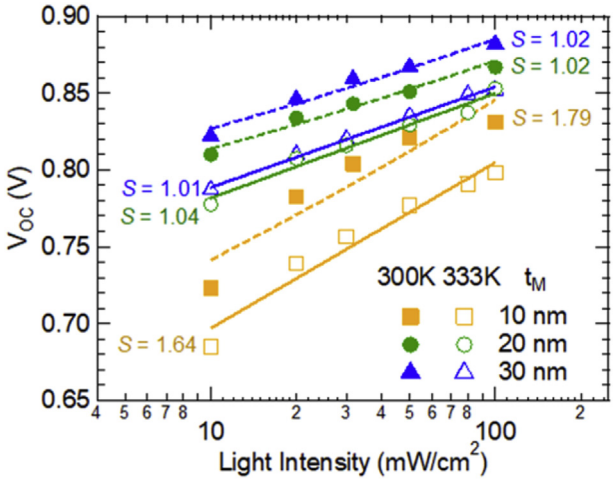

Fig. 7. V_{OC} of OSCs employing NS with different t_M as a function of light intensity.

(0.50) and 10 (0.58) are reduced and thereby PCE of them are significantly deteriorated. Meanwhile, in the cases with NS-20 and 30, photo generated carriers effectively move to electrode with small losses from the leakage, resulting in better PCE compared to their corresponding reference devices. Hence, distinct electrical features of NS with fully covered NPs compared to core/shell type NPs, to enhance carrier extraction without increasing leakage, lead to the improvement in PCE of OSC with NS, while the increased exciton generation and carrier extraction of OSCs with partially covered NPs are negated by leakage losses.

3.6. Carrier transport: recombination losses

For a more detailed study, we measured the impedance spectroscopy to analyse the carrier recombination in the device incorporating NS with different t_M. Fig. 6 shows the dependence of capacitance versus voltage (C–V) characteristics in OSCs with NS under dark condition. With a fixed thickness of polymer layer (~100 nm), the capacitance of devices embedding NS-20 and 30 is higher than that with NS-10. Here, the slope of C–V characteristics was utilized to estimate the carrier density (NC) based on Mott-Schottky model [35,36]. The calculated NC of OSCs including NS-10 (9.8×10^{16}/cm^3) is lower than those of NS-20 (5.1×10^{17}/cm^3) and 30 (3.8×10^{17}/cm^3), which are in the same range as the previous study on device with PCDTBT: $PC_{70}BM$ fabricated on flat buffer layer [35]. However, this model is not well matched with the cases of NS-5 because of its highly non-ideal diode behaviour caused by the high leakage current. Generally, NC is determined by excess carrier arising from the change of depletion region width, which is affected by injection, generation, and annihilation of carriers [37]. In this study, the photo-induced carrier generation in the active layer is negligible because this analysis was conducted under dark condition, and the interface for carrier injection and the energy level difference between donor and acceptor materials were maintained the same among all the devices. Thus, the decreased NC in the device with partially covered NPs might be attributed to the recombination losses of injected carrier. We believe that these partially covered NPs work as recombination centres that increase losses and decrease NC inside the active layer.

To establish how these traps contribute to the device performance under illumination, the semi-log incident light intensity (P_{Light}) dependence of V_{OC} for each sample was conducted at 300 K and 333 K as shown in Fig. 7. According to the previous research, Langevin recombination loss is dominant when a slope of P_{Light}- V_{OC} (s) is near thermal energy (K_BT/q), where K_B is Boltzman constant, T is absolute temperature, and q is a charge of single electron [17,38]. Meanwhile, the higher slope indicates the device performance is governed by trap-assisted (Schokley-Read-Hall) recombination. At room temperature, much steeper P_{Light}-V_{OC} slope is observed in the device with NS-10 ($s = 1.79 \cdot K_BT/q$), whereas these of NS-20 ($s = 1.02 \cdot K_BT/q$) and 30 ($s = 1.02 \cdot K_BT/q$) embedded devices are similar to the thermal energy. These results indicate that the photo-generated carriers in *OSCs* with NS-10, containing partially covered NPs, are recombined with their counter carriers captured in traps, while the holes effectively move to counter electrodes with small losses in the devices with NS-20 and 30 fully enclosing NPs. So, it is apparent that NPs directly contacted with the active polymer act as trap sites with increasing recombination losses under illumination as well as dark condition. Additionally, the decreased slope of device casted on NS-10 ($s = 1.64 \cdot K_BT/q$) at higher temperature (333 K) is another supportive evidence to explain the relation between NPs' encapsulated status and recombination characteristic because the possibility of releasing carriers captured in traps increases with raised thermal energy. In contrast, the slopes of cases with NS-20 and 30 are almost the same as the value at room-temperature regardless of increased thermal energy. Such trap assisted recombination losses prevent carriers from effectively transporting to electrodes in devices, so that the lower device performance of samples with NS-5 and 10 is exhibited. Moreover, it is observed that the device performance of OSCs with partially covered NPs is degraded as the light intensity diminishes (See Fig. S4). These can be ascribed to that most of the photo-generated carrier in low light intensity (20 mW/cm^2) is used to fill up the trap sites, which leads to remarkably reduced PCE of OSCs. On the other hand, the PCE of devices containing NS-20 and 30 are independent on the light intensity, revealing the small losses during extraction process. Therefore, our optical and electrical analyses reveal that the NS fully covering NPs in OSCs enhance carrier extraction without changing losses, while the increased carrier annihilation by trap-assisted leakage losses in partially covered NPs deteriorates the device performance.

4. Conclusion

We have analysed the effect of NS, consisting of 5–30 nm-thick MoO_3 and 40 nm-size Ag NPs, on the performance of PCDTBT:$PC_{70}BM$ solar cells. The PCE of OSCs embedding the oval-shape NS with t_M of 20–30 nm is improved and the best performance is achieved at t_M of 20 nm, whereas the devices with partially uncovered Ag NP by a thin t_M of 5–10 nm show lower efficiency compared to the devices with flat MoO_3 layer. The observed improvements are attributed to enhanced

exciton generation and improved carrier extraction by the NS-induced plasmonic effect and the undulated surface of active layer. The degraded performance of device including NS with the partially disclosed NPs is caused by the short lifetime of exciton, the trap-assisted recombination, and leakage loss. As a result, our systematic analysis of the NS on plasmonic OSCs allows one to optimize the device performance through both the optical and electrical enhancements.

Authorship of this work

Hyung-Jun Song: Conceptualization, Data curation, Formal analysis, Investigation, Methodology, Roles/Writing - original draft.

Gunhee Lee: Conceptualization; Data curation, Formal analysis, Investigation, Methodology, Roles/Writing - original draft.

Kinam Jung: Data curation; Formal analysis, Investigation; Methodology, Visualization.

Min Seok Jang: Investigation, Methodology, Writing - review & editing.

Jiho Sohn: Data curation.

Jong-Kwon Lee: Supervision, Writing - review & editing.

Mansoo Choi: Project administration, Funding acquisition, Supervision, Validation, Writing - review & editing.

Changhee Lee: Project administration, Funding acquisition, Supervision, Validation, Writing - review & editing.

Acknowledgements

This work was supported by the Global Frontier R&D Program on Center for Multiscale Energy System funded by the National Research Foundation under the Ministry of Science and ICT of Korea (2012M3A6A7054855).

Appendix A. Supplementary data

Supplementary data to this article can be found online at https://doi.org/10.1016/j.orgel.2019.05.007.

References

[1] J. Hou, O. Inganäs, R.H. Friend, F. Gao, Nat. Mater. 17 (2018) 119.
[2] D. Baran, R.S. Ashraf, D.A. Hanifi, M. Abdelsamie, N. Gasparini, J.A. Röhr, S. Holliday, A. Wadsworth, S. Lockett, M. Neophytou, C.J.M. Emmott, J. Nelson, C.J. Brabec, A. Amassian, A. Salleo, T. Kirchartz, J.R. Durrant, I. McCulloch, Nat. Mater. 16 (2017) 363.
[3] D.E. Markov, E. Amsterdam, P.W.M. Blom, A.B. Sieval, J.C. Hummelen, J. Phys. Chem. A 109 (2005) 5266.
[4] H.A. Atwater, A. Poleman, Nat. Photon. 9 (2010) 205.
[5] P. Mandal, S. Sharma, Renew. Sustain. Energy Rev. 65 (2016) 537.
[6] L. Lu, M.A. Kelly, W. You, L. Yu, Nat. Photon. 9 (2015) 491.
[7] J. Yang, J. You, C.-C. Chen, W.-C. Hsu, H.-R. Tan, X.W. Zhang, Z. Hong, Y. Yang, ACS Nano 5 (2011) 6210.
[8] Q. Gan, F.J. Bartoli, Z.H. Kafafi, Adv. Mater. 25 (2013) 2385.
[9] E. Stratakis, E. Kymakis, Mater. Today 16 (2013) 133.
[10] T. Fleetham, J.-Y. Choi, H.W. Choi, T. Alford, D.S. Jeong, T.S. Lee, W.S. Lee, K.-S. Lee, J. Li, I. Kim, Sci. Rep. 5 (2015) 14250.
[11] K. Jung, H.-J. Song, G. Lee, Y. Ko, K. Ahn, H. Choi, J.Y. Kim, K. Ha, J. Song, J.-K. Lee, C. Lee, M. Choi, ACS Nano 8 (2014) 2590.
[12] J.M. Lee, J. Lim, N. Lee, H.I. Park, K.E. Lee, T. Jeon, S.A. Nam, J. Kim, J. Shin, S.O. Kim, Adv. Mater. 27 (2015) 1519–1525.
[13] S. Liu, R. Jiang, P. You, X. Zhu, J. Wang, F. Yan, Energy Environ. Sci. 9 (2016) 898.
[14] S. Kim, C.-H. Kim, S.K. Lee, J.-H. Jeong, J. Lee, S.-H. Jin, W.S. Shin, C.E. Song, J.-H. Choi, J.-R. Jeong, Chem. Commun. 49 (2013) 6033.
[15] D. Knipp, V. Jovanov, A. Tamang, V. Wagner, A. Salleo, Nanomater. Energy 31 (2017) 582.
[16] M. Xue, L. Li, B.J.T. de Villers, H. Shen, J. Zhu, Z. Yu, A.Z. Stieg, Q. Pei, B.J. Schwartz, K.L. Wang, Appl. Phys. Lett. 98 (2011) 253302.
[17] B. Wu, X. Wu, C. Guan, K. Fai Tai, E.K.L. Yeow, H. Jin Fan, N. Mathews, T.C. Sum, Nat. Commun. 4 (2013) 2004.
[18] K.S. Nalwa, J.-M. Park, K.-M. Ho, S. Chaudhary, Adv. Mater. 23 (2011) 112.
[19] J. Wang, Y.-J. Lee, A.S. Chadha, J. Yi, M.L. Jespersen, J.J. Kelley, H.M. Nguyen, M. Nimmo, A.V. Malko, R.A. Vaia, W. Zhou, J.W.P. Hsu, J. Phys. Chem. C 117 (2012) 85.
[20] M. Salvador, B.A. MacLeod, A. Hess, A.P. Kulkarni, K. Munechika, J.I.L. Chen, D.S. Ginger, ACS Nano 6 (2012) 10024.
[21] V. Janković, Y. Yang, J. You, L. Dou, Y. Liu, P. Cheung, J.P. Chang, Y. Yang, ACS Nano 7 (2013) 3815.
[22] H. Choi, J.-P. Lee, S.-J. Ko, J.-W. Jung, H. Park, S. Yoo, O. Park, J.-R. Jeong, S. Park, J.Y. Kim, Nano Lett. 13 (2013) 2204.
[23] H.G. Scheibel, J. Porstendörfer, J. Aerosol Sci. 14 (1983) 113.
[24] M.H. Magnusson, K. Deppert, J.–O. Malm, J.–O. Bovin, L. Samuelson, J. Nano Res. 1 (1999) 243 1999.
[25] H. Kim, J. Kim, H.J. Yang, J. Suh, T. Kim, B.W. Han, S. Kim, D.S. Kim, P.V. Pikhitsa, M. Choi, Nat. Nanotechnol. 1 (2006) 117.
[26] J. C Ostrowski, A. Mikhailovsky, D.A. Bussian, M.A. Summers, S.K. Buratto, G.C. Bazan, Adv. Funct. Mater. 16 (2006) 1221.
[27] H. Chew, J. Chem. Phys. 87 (1987) 1355.
[28] S.-S. Kim, S.-I. Na, J. Jo, D.-Y. Kim, Y.-C. Nah, Appl. Phys. Lett. 93 (2008) 073307.
[29] B. Wu, T.Z. Oo, X. Li, X. Liu, X. Wu, E.K.L. Yeow, H.J. Fan, N. Mathews, T.C. Sum, J. Phys. Chem. C 116 (2012) 14820.
[30] J.-L. Wu, F.-C. Chen, Y.-S. Hsiao, F.-C. Chien, P. Chen, C.-H. Kuo, M.H. Huang, C.-S. Hsu, ACS Nano 5 (2011) 959.
[31] Z. Su, L. Wang, Y. Li, G. Zhang, H. Zhao, H. Yang, Y. Ma, B. Chu, W. Li, ACS Appl. Mater. Interfaces 5 (2013) 12847.
[32] A. Moliton, J.–M. Nunzi, Polym. Int. 55 (2006) 583.
[33] S. Noh, C.K. Suman, D. Lee, S. Kim, C. Lee, J. Nanosci. Nanotechnol. 10 (2010) 6815.
[34] H. Liu, W.-P. Goh, M.Y. Leung, Y. Li, T.B. Norsten, Sol. Energy Mater. Sol. Cells 96 (2012) 302.
[35] W. Brütting, H. Riel, T. Beierlein, W. Riess, J. Appl. Phys. 89 (2001) 1704.
[36] P.P. Boix, G. Garcia-Belmonte, U. Muñecas, M. Neophytou, C. Waldauf, R. Pacios, Appl. Phys. Lett. 95 (2009) 233302.
[37] Y. Zhang, H. Zhou, J. Seifter, L. Ying, A. Mikhailovsky, A.J. Heeger, G.C. Bazan, T.-Q. Nguyen, Adv. Mater. 25 (2013) 7038.
[38] M.M. Mandoc, F.B. Kooistra, J.C. Hummelen, B. de Boer, P.W.M. Blom, Appl. Phys. Lett. 91 (2007) 263505.